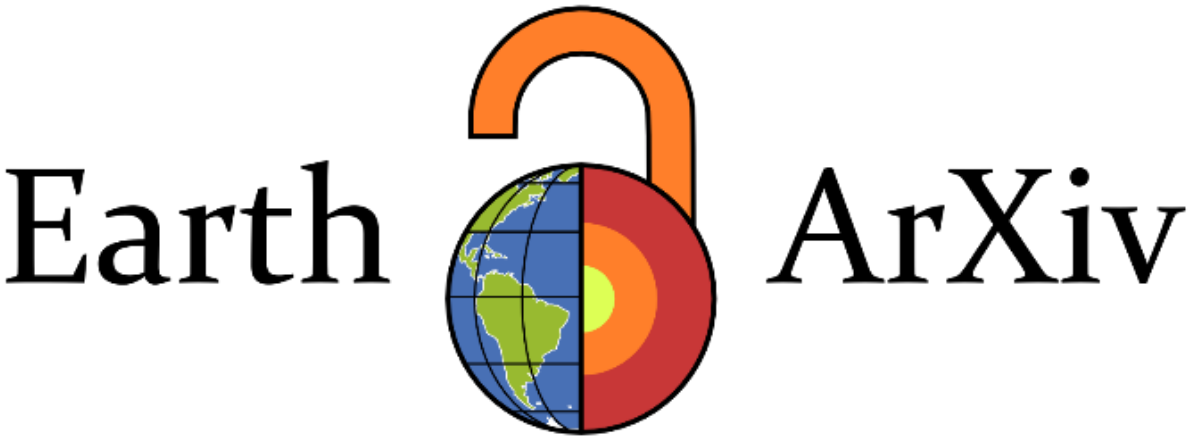

Development of a dynamic true triaxial electromagnetic Hopkinson bar system

Heping Xie[1,2], Jianbo Zhu[1,2*], Yulong Li[3*], Tao Zhou[1,2*], Shiwei Zhang[1,2], Weiyue Bao[1,2], Zhongbin Tang[3], Tao Suo[3], Xiaoyong Song[1,2], Jian Zhao[4]

[1] State Key Laboratory of Intelligent Construction and Healthy Operation and Maintenance of Deep Underground Engineering, College of Civil and Transportation Engineering, Shenzhen University, Shenzhen, 518060, China

[2] Guangdong Provincial Key Laboratory of Deep Earth Sciences and Geothermal Energy Exploitation and Utilization, Institute of Deep Earth Sciences and Green Energy, College of Civil and Transportation Engineering, Shenzhen University, Shenzhen, 518060, China

[3] School of Aeronautics, Northwestern Polytechnical University, 127 Youyi West Road, Xi'an 710072, China

[4] Department of Civil Engineering, Monash University, Melbourne, VIC 3800, Australia

* Corresponding authors; Emails: jianbo.zhu@szu.edu.cn, liyulong@nwpu.edu.cn, tzhou@szu.edu.cn

Peer review status:

This is a non-peer-reviewed preprint submitted to EarthArXiv.

This preprint has been submitted for consideration to the International Journal of Rock Mechanics and Mining Sciences, where it is currently undergoing peer review.

Development of a dynamic true triaxial electromagnetic Hopkinson bar system

Heping Xie[1,2], Jianbo Zhu[1,2]*, Yulong Li[3]*, Tao Zhou[1,2]*, Shiwei Zhang[1,2], Weiyue Bao[1,2], Zhongbin Tang[3], Tao Suo[3], Xiaoyong Song[1,2], Jian Zhao[4]

[1] State Key Laboratory of Intelligent Construction and Healthy Operation and Maintenance of Deep Underground Engineering, College of Civil and Transportation Engineering, Shenzhen University, Shenzhen, 518060, China

[2] Guangdong Provincial Key Laboratory of Deep Earth Sciences and Geothermal Energy Exploitation and Utilization, Institute of Deep Earth Sciences and Green Energy, College of Civil and Transportation Engineering, Shenzhen University, Shenzhen, 518060, China

[3] School of Aeronautics, Northwestern Polytechnical University, 127 Youyi West Road, Xi'an 710072, China

[4] Department of Civil Engineering, Monash University, Melbourne, VIC 3800, Australia

* Corresponding authors; Emails: jianbo.zhu@szu.edu.cn, liyulong@nwpu.edu.cn, tzhou@szu.edu.cn

Abstract: Subsurface rock masses and rock engineering are subjected to multiaxial static stresses and often also bear additional multi-directional dynamic disturbances generated by seismic activity, blast waves and vibration, etc. It is therefore of great importance to study and understand the dynamic mechanical behaviors and failure mechanisms of rocks under multiaxial and multidirectional dynamic disturbances for the scientific design, safe construction and stable operation of rock engineering. In view of this, a novel dynamic true triaxial electromagnetic Hopkinson bar (DTEHB) system is proposed and developed in this paper. It offers a cutting-edge testing platform for studying dynamic responses of rock masses, taking into account the coupled effects of three-dimensional dynamic disturbances with strain rates ranging from 10^1 s^{-1} to 10^3 s^{-1} and triaxial static in situ stresses. The fundamental principles, configuration and the technical challenges associated with the development of the DTEHB are introduced in detail. The viability and effectiveness of DTEHB were verified through an analysis of measured controllable and adjustable stress waveform data and an evaluation of dynamic true triaxial synchronized impact test results on coal specimens. The establishment of the DTEHB will facilitate experimental testing of rock and other materials under a range of dynamic disturbances, thereby advancing the theory of three-dimensional rock dynamic theories and its application in geotechnical engineering.

Keywords： Rock dynamics; DTEHB; Dynamic true triaxial loading; Synchronous control

1. Introduction

As demands for energy and the exploitation and utilization of resources, as well as transportation development, continue to grow, the number of rock engineering projects under construction or about to be built in areas with active dynamic disturbances and a deep earth with high and more complicated crustal stresses is also increasing. In such locations, the subsurface rock masses and rock engineering are subjected to triaxial static stresses and often bear additional multi-axial and multi-directional dynamic disturbances generated by factors such as earthquake, blast and vibration. As a result, abrupt and unpredictable dynamic hazards, including rockbursts, coal bumps and large-scale caving, occur with considerable frequency during the construction and operation of those rock structures (Ranjith et al. 2017; Rehbock-Sander and Jesel 2018; Xie et al. 2019, 2020). In light of the risk of dynamic disasters and the difficulty in their prediction and prevention, it is of great importance to gain a comprehensive understanding of rock dynamics, taking into account the multi-axial and multi-directional dynamic and static stresses.

As a fundamental and practical method, laboratory experiments have been widely applied to study dynamic mechanical and deformational behaviors of rock materials subjected to dynamic impacts. To date, there are several techniques have been utilized to investigate rock dynamic behaviors at different strain rates, e.g., the hydraulic/stress servo-control apparatus (Fairhurst and Hudson 1999; Olsson 1991), the drop weight device (Reddish et al. 2005; Whittles et al. 2006), the split Hopkinson bar (SHB) (Kolsky 1963; Zhao and Gary 1996) and the planar impact machine (Ahrens and Rubin 1993). Among them, the SHB is the most widely employed for testing rock dynamics at intermediate to high strain rates (10^1~10^3 s^{-1}).

The SHB for rock dynamics characterization was first introduced by Kumar in 1968 (Kumar 1968) and has since been applied extensively (Doan and Gary 2009; Frew et al. 2001; Goldsmith et al. 1976; Ju et al. 2007; Lambert and Ross 2000; Li et al. 2005, 2017a, 2017b; Lindholm et al. 1974; Lu et al. 2010; Melosh et al. 1992; Olsson 1991; Perkins et al. 1970; Qi et al. 2019; Wang et al. 2009, 2017, 2018; Wu et al. 2016; Xia and Yao 2015; Xie and Sanderson 1996; Yuan et al. 2011; Zhang and Zhao 2013, 2014; Zhou et al. 2018, 2020; Zhu et al. 2018a). Attributed to those studies, it is commonly recognized that the mechanical and cracking behaviors of rock materials are strain rate dependent. As previously stated, rocks are usually subjected to the combined influences of

static *in situ* stresses and dynamic disturbances. It is, however, impossible to mimic such kind of the stress conditions using the conventional SHB. To address this technical issue, significant effort has been devoted in recent years. In a pioneering modification of the SHB, Li et al. (2008) devised an axisymmetric triaxial confined SHB apparatus, wherein a dynamic load is applied from one direction and static axisymmetric triaxial confined stresses ($\sigma_1 \geqslant \sigma_2 = \sigma_3 \neq 0$, where σ_1, σ_2 and σ_3 are principal stresses) are loaded to the specimen. Additionally, static axisymmetric triaxial confined stresses can also be achieved by incorporating a transverse constraint ring around the specimen during dynamic loading along the axial direction (Chen and Ravichandran 1997; Chen and Song 2011). To achieve a true triaxial stress state ($\sigma_1 \geqslant \sigma_2 \geqslant \sigma_3 \neq 0$) on rock samples prior to dynamic impact, Zhao and Cadoni (2009) proposed a modified SHB conception that can initially load the rock specimen to a static true triaxial stress state before impacting along one direction. However, this conception has not yet been put into practice. In a recent development, Liu et al. (2019) constructed a triaxial Hopkinson bar, which was then employed in an investigation into the dynamic behavior of sandstone specimens under static true triaxial confinements and dynamic loading from a single direction.

Nevertheless, it is not yet possible to apply any of the existing SHB systems to perform dynamic tests with true triaxial impact. In fact, rocks and rock-like materials may encounter multi-axial and multi-directional impacts which could be synchronous or asynchronous, of equal or unequal magnitude in different directions. For example, in shaft excavation and mining using the drilling and blasting method, rocks located at the center of the spiro-arranged holes are often subjected to multi-axial and multi-directional (e.g., symmetric, biaxial/four-directional or triaxial/six-directional) blasting waves that arrive at different times and vary along different directions. In the context of ballistic impact and penetration, the protective rock and concrete structures would bear multi-axial dynamic loads (Karinski et al. 2017; Luo et al. 2019). Therefore, it is essential to develop an innovative dynamic testing system that is able to apply controllable true triaxial impacts on rock specimens.

In this paper, the development of a dynamic true triaxial electromagnetic Hopkinson bar (DTEHB) is introduced, with the aim to provide an innovative dynamic testing platform for the characterization of rock dynamics subjected to the combined influences of three-dimensional (3D) dynamic and *in-situ* static stress with strain rates ranging from 10^1 s^{-1} to 10^3 s^{-1}. The fundamental

principles, configuration and the technical challenges associated with the development of the DTEHB are introduced in detail. The viability and effectiveness of DTEHB are verified through experimental testing. The establishment of the DTEHB will facilitate the advancement of the theory of 3D rock dynamics and its application in geotechnical engineering.

2. State of the Art of Split Hopkinson Bar

A conventional SHB is comprised of four principal components: a striker, an input bar, an output bar and a buffer bar. During testing, the specimen is positioned between the input and output bars. Upon impact with the end of the input bar by the striker, a stress wave is generated, which propagates along the input bar. Upon reaching the interface between the input bar and the specimen, a portion of the stress wave passes through the specimen and then propagates into the output bar as a transmitted stress wave, while the remaining part is reflected back into the input bar as a reflected stress wave. Typically, the strain signals in the bars are recorded by means of resistance strain gauges affixed to the input and output bars. When dynamic force balance is attained at both ends of the specimen, the dynamic stress, strain and strain rate of the specimen can be calculated in accordance with the one-dimensional stress wave propagation theory and the methodology proposed by the ISRM (Zhou et al. 2012).

Although the SHB device has been widely applied to perform dynamic testing on various materials, it is, in fact, a technique that involves a certain degree of compromise rather than being an ideal solution. For instance, one of the fundamental assumptions of the SHB is that the dynamic stress across the entire specimen should be in equilibrium and that the specimen should deform uniformly (Chen and Song 2011; Kolsky 1963). This is because a lack of stress equilibrium across the specimen will result in the generation of inertial stress, which will consequently affect the magnitude of the transmitted wave as recorded in the output bar. The lack of stress equilibrium between specimen ends under dynamic compression may cause premature fracture of the brittle specimen (e.g., rock and concrete) at very low strains, and fracturing will result in a reduction in the amplitude of the transmitted wave (Lindholm et al. 1974). Although the pulse shaping technique is usually adopted to modify the conventional trapezoidal incident pulse into a half sine wave with a prolonged and slowly rising wave front, thereby facilitating stress balance in the specimen (Frew et

al. 2002; Li et al. 2009; Song and Chen 2004), the stress equilibrium still cannot be fully achieved as the incident pulse needs to transmit from one end to the other end of the specimen to gradually reach stress equilibrium (Frew et al. 2002). Furthermore, the inability to precisely control the pulse shaping or the conventional pneumatic launching technique results in an inherent lack of repeatability in the generated incident pulses, even when the launching gas pressure is maintained constant.

In the conventional SHB testing, the incident stress pulse is usually generated by a mechanical process, e.g., the impact of the striker (Chen and Song 2011) or a sudden release of a pre-tensioned bar section (Cadoni et al. 2009). This makes it challenging to generate multiple incident stress pulses simultaneously, which is necessary for multi-axial and multi-directional synchronized impact testing. As a consequence, the majority of existing SHBs are only capable of achieving dynamic impact along a single direction. In a recent report, Nie et al. (2018b) proposed a symmetric loading SHB apparatus that employs the electromagnetic energy conversion technique, with which a single-axial and bidirectional synchronous compression or tension test can be performed.

Almost all of the so-called triaxial SHB instruments can only apply static axisymmetric triaxial confined stresses ($\sigma_1 \geqslant \sigma_2 = \sigma_3 \neq 0$) to the test specimens (Chen and Song 2011; Frew et al. 2002; Gran et al. 1989; Gary and Bailly 1998; Hokka et al. 2016; Li et al. 2008; Nemat-Nasser et al. 2000; Yuan et al. 2011; Peng et al. 2019), except the true triaxially compressed SHB proposed by Zhao and Cadoni in 2009 (Zhao and Cadoni 2009; Cadoni and Albertini 2011), and fully built at Monash University in 2017 (Zhao et al 2015; Liu et al. 2019), which could apply true triaxial static confining pressures. Moreover, with increasing depth of the underground engineering, rocks are affected by thermal effects. Nevertheless, there is currently no laboratory apparatus that has been developed to study the coupled effects of real-time thermal treatment and dynamic and static triaxial stresses.

It is therefore essential to develop an innovative 3D dynamic testing device that is capable of repeatably generating stress waves according to the required specifications, accurately controlling the arrival time of the multiple stress waves from different directions, and achieving the coupled influence of true triaxial synchronous impacts and *in situ* static stresses. This will overcome the limitations of the present SHB technique.

3. Design and Configuration of the DTEHB System

To address the challenges associated with 3D dynamic response and the mechanism of dynamic disasters during construction and operation of major rock structures, and to overcome the shortcomings of the existing SHB technique, we propose the development of the DTEHB. This technique is capable of achieving dynamic true triaxial loading and enables the control, adjustment, and repetition of dynamic stress loading. Fig. 1 demonstrates the DTEHB, which is mainly composed of a controllable pulse generation and loading system, a true triaxial servo-controlled confining pressure loading system, an orthogonal triaxial arrangement of bar and frame system, and a data acquisition and analysis system. With these functions, the DTEHB can be utilized to investigate the dynamic behaviors and failure mechanisms of various materials, including rock, hard soil, concrete, ceramics, composites, polymers, energy-absorbing materials, and aerospace materials, under triaxial dynamic impacts (e.g., from symmetric loading to biaxial/four-directional and triaxial/six-directional loading), with due consideration of the *in-situ* conditions.

3.1 Principle of the DTEHB

Fig. 2 illustrates the schematic diagram of the stress state and wave propagation in the triaxial bars. The specimen is under the combined influences of static triaxial confining pressures ($\sigma_x \neq \sigma_y \neq \sigma_z \neq 0$) and dynamic true triaxial impacts. Notably, the static triaxial confining stresses are loaded to the specimen before applying dynamic true triaxial impacts. As depicted in Fig. 2, the stress waves applied in the true triaxial impact test (i.e., $\varepsilon_{x\text{-}inc}$, $\varepsilon_{y\text{-}inc}$ and $\varepsilon_{z\text{-}inc}$) can propagate synchronously and symmetrically along the corresponding bars and the specimen. When the specimen is subjected to synchronous and symmetrical impacts along six directions, three stress waves, i.e., reflected waves, transmitted waves and elastic waves induced by Poisson's effect, will be generated along each axial direction. Although these three waves are superposed into a single waveform, the propagation of the superposed wave in each axial direction still follows the one-dimensional elastic wave propagation theory (Cadoni and Albertini 2011). Furthermore, the propagation of two identical stress waves symmetrically into the bars ensures that the dynamic force balance of the specimen along the loading direction can be well achieved during the dynamic loading process. Accordingly, the one-dimensional elastic wave propagation theory can still be used

to analyze dynamic responses of the specimen in dynamic true triaxial impact loading tests.

To further clarify wave propagation in the DTEHB, an *x*-*t* diagram of the propagation of waves along the *x*-axis under conditions of symmetric loading is illustrated in Fig. 3. Two identical incident waves propagate simultaneously and symmetrically from the ends of the right and left incident bars toward the specimen. In this context, the incident waves originating from the right and left are defined as ε_{inc_right} (right incident wave) and ε_{inc_left} (left incident wave), respectively. In general, when a stress wave reaches the interface between the input bar and the specimen, a portion of the stress wave passes through the specimen and then propagates into the output bar as a transmitted stress wave. The remaining portion of the stress wave is reflected back into the input bar as a reflected stress wave. As shown in Fig. 3, upon reaching the right interface between the input bar and specimen, a portion of the stress wave is reflected, while the remainder transmits through the specimen and into the left input bar. Likewise, the right-travelling wave in the left input bar propagates according to the aforementioned principle. Given that the time required for the wave to propagate within the specimen is considerably shorter than the duration of the incident wave, the initial arrival wave in the right input bar can be regarded as a superposition of the reflected wave from the right incident wave and the transmitted wave from the left incident wave, which is labelled as ε_{ref_right}. Similarly, the initial arrival wave in the left input bar is also a superposition of two parts and is designated as ε_{ref_left}.

To avoid superposition of the incident and reflected waves in each bar, the two pulses are recorded by the resistance strain gauges mounted at midpoints along the length of the bars. Because the square bar is a slender bar and the incident wave is a half sine wave with weak high-frequency components, the waveform dispersion and oscillation are negligible. Thus, in accordance with the one-dimensional stress wave theory (Kolsky 1963), the dynamic forces (P) and particle velocities (V) at the right and left ends of the specimen can be calculated as follows:

$$P_{left} = AE(\varepsilon_{inc\_left} + \varepsilon_{ref\_left}),\ P_{right} = AE(\varepsilon_{inc\_right} + \varepsilon_{ref\_right}) \tag{1}$$

$$V_{left} = C(\varepsilon_{inc\_left} - \varepsilon_{ref\_left}),\ V_{right} = C(-\varepsilon_{inc\_right} + \varepsilon_{ref\_right}) \tag{2}$$

where C, A and E are the P-wave velocity, cross-section area and elastic modulus of the input bar, respectively.

Given that the right and left incident waves are identical and symmetrically loaded, it is

feasible to maintain dynamic stress equilibrium effectively throughout the dynamic loading process. Therefore, the dynamic stress of the specimen can be characterized by the average stress on both sides of the specimen. Based on the one-dimensional stress wave theory (Kolsky 1963), the dynamic stress $\sigma(t)$, the strain rate $\dot{\varepsilon}(t)$ and dynamic strain $\varepsilon(t)$ of the specimen in dynamic impact along each axial direction can be computed as follows (Nie et al. 2018b; Xie et al. 2021):

$$\sigma(t)=\frac{\sigma_{left}+\sigma_{right}}{2}=\frac{1}{2}\frac{A}{A_s}E(\varepsilon_{inc\_left}+\varepsilon_{inc\_right}+\varepsilon_{ref\_left}+\varepsilon_{ref\_right}) \tag{3}$$

$$\dot{\varepsilon}(t)=\frac{V_{left}-V_{right}}{L_s}=\frac{C}{L_s}(\varepsilon_{inc\_left}+\varepsilon_{inc\_right}-\varepsilon_{ref\_left}-\varepsilon_{ref\_right}) \tag{4}$$

$$\varepsilon(t)=\int_0^t\dot{\varepsilon}dt=\frac{C}{L_s}\int_0^t(\varepsilon_{inc\_left}+\varepsilon_{inc\_right}-\varepsilon_{ref\_left}-\varepsilon_{ref\_right})dt \tag{5}$$

where L_s and A_s are the length and cross-section area of the specimen, respectively.

Because the strength of the rock and rock-like materials significantly increases with increasing confining pressure (Patton et al. 1998; Richter et al. 2018; Wasantha and Ranjith 2014; Zhu et al. 2016), and rock brittle failure switches to ductile one under high confining pressure (Kumari et al. 2017; Peng et al. 2015; Scott and Nielsen 1991). The Von Mises stress may be employed for the evaluation or analysis of the dynamic deformation and failure of the specimen subjected to the combined effect of dynamic true triaxial impacts and static triaxial stresses. The equivalent stress ($\bar{\sigma}$) and equivalent strain ($\bar{\varepsilon}$) of the specimen under the combined influence of triaxial static pressures and dynamic true triaxial impacts can be calculated as follows (Xu et al. 2020):

$$\bar{\sigma}=\sqrt{\frac{1}{2}[(\sigma_{x\_dyn}+\sigma_{x\_static}-\sigma_{y\_dyn}-\sigma_{y\_static})^2+(\sigma_{y\_dyn}+\sigma_{y\_static}-\sigma_{z\_dyn}-\sigma_{z\_static})^2+(\sigma_{z\_dyn}+\sigma_{z\_static}-\sigma_{x\_dyn}-\sigma_{x\_static})^2]} \tag{6}$$

$$\bar{\varepsilon}=\sqrt{\frac{2}{9}[(\varepsilon_{x\_dyn}+\varepsilon_{x\_static}-\varepsilon_{y\_dyn}-\varepsilon_{y\_static})^2+(\varepsilon_{y\_dyn}+\varepsilon_{y\_static}-\varepsilon_{z\_dyn}-\varepsilon_{z\_static})^2+(\varepsilon_{z\_dyn}+\varepsilon_{z\_static}-\varepsilon_{x\_dyn}-\varepsilon_{x\_static})^2]} \tag{7}$$

where σ_{i_dyn}, σ_{i_static}, ε_{i_dyn} and ε_{i_static} represent dynamic stress, static confining pressure, dynamic strain and static strain corresponding to the peak static confining pressure along the *i*-axis (*i*=*x*, *y*, and *z*).

3.2 Configuration of the DTEHB

As aforementioned, the DTEHB is able to realize multi-axial and multi-directional

synchronous or asynchronous loading (e.g., from 1D symmetric loading to biaxial/four-directional and triaxial/six-directional loading), dynamic-static coupled loading, controllable and repeatable dynamic impact. As illustrated in Fig. 1, the DTEHB consists of a triaxial frame, an orthogonal bar set, a stress wave launching system, a static triaxial confining pressure system and a data acquisition and analysis system.

The triaxial frame is a 3D symmetric frame structure with sufficiently high stiffness. To achieve true triaxial loading, the bar is designed with a square cross-section. In the DTEHB, three pairs of orthogonal square bars with circular bulges constitute the 3D dynamic impact loading bar system, as shown in Fig. 2. The static confining pressure loading system is a servo-controlled and triaxial. The servo-controlled system enables the independent application of true triaxial static confining pressure to the specimen, either in identical or different magnitudes, thus simulating the *in-situ* static stress conditions. The true triaxial static confining pressure can be maintained at a relatively constant level by the servo-controlled system during the dynamic loading process, thus preventing the occurrence of apparent oscillations in the confining pressure induced by the Poisson's effect during dynamic loading.

The stress wave launching system is comprised primarily of an electromagnetic stress pulse generation system and a synchronized control system (SCS). Through a collaborative process of involving the electromagnetic stress pulse generators (ESPGs) and the SCS, electric energy is converted into electromagnetic pulses, which are subsequently transmitted to the elastic bars in the form of stress waves. Since the capacitance and charging voltage of the ESPG are adjustable, both the electromagnetic stress pulse duration and amplitude are controllable and adjustable. Furthermore, the high precision of the SCS ensures the stability and repeatability of the electromagnetic stress pulses. Moreover, the SCS enables the precise synchronous generation of electromagnetic stress pulses by the ESPGs, thus guaranteeing the capability to perform multi-axial and multi-directional impact loading (e.g., 1D symmetric loading, biaxial and four-directional loading, and triaxial and six-directional loading) in a synchronous or asynchronous manner.

It is crucial to ensure the accurate acquisition and analysis of testing data, as the success of dynamic testing depends on the ability to capture and distinguish the actual test data from the surrounding noise. It is therefore essential that the test data reflecting the dynamic mechanical characteristics and damage and fracture behaviors, e.g., strain signals, acoustic emission and

fracturing process, of the specimen during dynamic loading are effectively captured. In light of this, the DTEHB incorporates a range of integrated techniques, including contact and non-contact data measurement, real-time monitoring and post-test analysis tools, macro and micro characterization techniques, and both nondestructive and destructive methods. These are collectively employed for the observation, collection and analysis of test data. Table 1 provides a summary of the techniques and equipment utilized in the DTEHB, along with the objectives of data acquisition and results analysis with the aforementioned equipment. Notably, the digital image correlation technique and the ultra-high-speed camera are employed to capture and analyze surface dynamic fracturing behavior under all loading conditions (e.g., 1D symmetric loading, and biaxial/four-directional loading) with the exception of true triaxial dynamic loading. In a true triaxial dynamic test, the specimen is completely buried by six opaque bars, so that no surface is available for the image-based techniques to capture the deformation and fracture of the specimen.

4. Technical Challenges Addressed in the Development of the DTEHB

To fulfill the functions of the DTEHB, the following technical challenges have been addressed: the development of a technique for producing targeted stress waves with high precision and repeatability; an approach for synchronously generating multiple identical stress waves with high consistency; a technique for controlling the loading of stress waves from different axes/directions with high synchronization (time difference within microseconds); the creation of an effective control system to coordinate the dynamic triaxial impact loading system; and the development of a servo-controlled triaxial static pressure loading system.

4.1 Dynamic Triaxial Impact Loading System

As aforementioned, one of the inherent limitations of the existing SHB devices is their inability to perform multi-axial and multi-directional synchronous or asynchronous impact loading tests with high precision and repeatability. This is because it is not feasible to achieve synchronization of the microsecond scale and controllable incident pulse with sufficiently precision and repeatability for multi-axial and multi-directional loading when the incident pulses are generated by the conventional mechanical means, such as impact by a striker or a sudden release of the pre-tensioned bar section (Nie et al. 2018a; Cadoni and Albertini 2011). To address this

technical issue, we propose an efficient approach that employs high precision and repeatability to generate multiple identical stress waves in a synchronous manner, using the electromagnetic energy conversion technique. The SCS allows for precise and repeatable synchronization of the stress wave generation and loading. The control system enables the electromagnetic stress pulse generation system to be operated automatically and safely. The integration of the electromagnetic energy conversion technique, the SCS and the control system allows for the realization of controllable true triaxial dynamic loading.

4.1.1 Electromagnetic Stress Pulse Generation System

The proposed DTEHB is composed of three sets of orthogonally assembled electromagnetic split Hopkinson bars, as shown in Fig. 1. The structure, principle and operation of the bar are identical along three axes (i.e., the X, Y and Z axes). Furthermore, the operation along each axis is independent and does not interfere with operation along the others. Therefore, only the structure, principle and operation of the electromagnetic Hopkinson bar along one axis are presented here.

The bar system, arranged along a single axis, comprises two ESPGs with active and inductive coils, two incident bars, and two charging circuits with symmetrically placement, as demonstrated in Fig. 4. The charging circuit, which is controlled by a thyristor, is connected to the corresponding ESPG. The charging circuit, consisting of a bridge rectifier and a high-power transformer, is applied to convert the alternating voltage (380V) into a targeted high direct voltage. A group of specialized pulse capacitors, either in series or parallel, is employed for energy storage during the charging process. The capacitor group, the active coil of the electromagnetic stress pulse generator and a thyristor form an LC circuit. During service, the two thyristors are activated simultaneously, enabling the discharge current generated by the fully charged capacitor groups to flow into two identical active coils in a uniform and simultaneously manner. Notably, the thyristor is a one-way conduction switch, which is adopted to permit the passage of the positive discharge current while preventing the reverse current from flowing. Then, the pulsed discharge current flows into the active coil, where it is converted into a stress pulse under the principle of electromagnetic conversion. Given the length of this article, a detailed description of the principles of electromagnetic conversion is beyond the scope of this paper. For further information on this topic, please refer to the work of Nie et al. (2018a).

To obtain repeatable and accurate electromagnetic stress pulses, it is essential that the ESPG, in particular the active coil, be designed with great care and precision. The structure and parameter design of a typical active coil are demonstrated in Fig. 5. The active coil has a diameter of 144 mm and a height of 58 mm. The core of the active coil is composed of a copper strip with a thickness of 4 mm and a height of 15 mm, wound in eight concentric circles in a configuration analogous to a "Swiss roll". Notably, to guarantee the precision of the machining process, the preparation of copper strips is accomplished through the use of wire cutting. The gap between two successive turn of copper strip is 2 mm, with an insulation rubber filled to prevent interlayer discharge. To resist the instant and powerful Lorentz force generated by the active coil in the perpendicular direction, a high-strength composite base has been designed to enhance the structural strength. Two copper strips protrude from the active coil and are designed as the positive and negative electrodes. An insulation block is fixed between the two electrodes to prevent short circuits.

Once the ESPG has been manufactured according to the design specifications, its inductance is determined. This is due to the factor that the inductance is directly proportional to the number of turns of copper strip in the active coil, and thus is not adjustable for a given pulse generator (Nie et al. 2018a). In accordance with the theory of an underdamped LRC circuit, the duration of the discharge current is, therefore, determined by the capacitance of the active coil and can be estimated as follows:

$$T = \pi\sqrt{LC_e} \tag{8}$$

where L and C_e are the inductance and capacitance of the active coil, respectively.

According to the principle of electromagnetic conversion, the influx of the discharge current into the active coil will, in time, give rise to the generation of a stress pulse by the Lorentz force at the surface of the inductive coil adjacent to the active coil. The duration of the pulse is directly related to the duration of the abrupt discharge current. In other words, the stress pulse duration is mainly determined by the capacitance of the active coil. Furthermore, a series of stress pulses with different durations can be generated by changing the capacitance through the addition or subtraction of parallel or series-connected capacitors, respectively.

In essence, the energy released by the discharge of the capacitor in an LC circuit is ultimately converted to the energy carried by the stress pulse via electromagnetic conversion. Consequently,

the energy of the electromagnetic stress pulse can be adjusted by changing the energy amplitude of the capacitor during the charging and discharging process. According to the discharge theory of LC circuits, the electric energy stored in the capacitor within an LC circuit can be calculated by

$$W_e = \frac{1}{2} C_e U^2 \tag{9}$$

where U is the charging voltage.

The utilization of the capacitor serves to regulate the duration of the pulse, thereby enabling the modification of the charging voltage in accordance with the specified pulse. This, in turn, allows for the control of the amplitude of the pulse. In accordance with the specifications, the wave amplitude is designed to fall within the range of 0 to 600 MPa, while the wave duration is set to a range of 300 to 800 μs.

4.1.2 Synchronous Control System

As aforementioned, the true triaxial dynamic testing device is composed of three sets of orthogonal symmetric Hopkinson bars, with the electromagnetic stress pulses applied to each symmetric Hopkinson bar being independently generated. It follows that the generation of incident stress pulses synchronously along the bars is essential for the realization of true triaxial dynamic impact loading. The challenge, therefore, is to determine how stress pulses can be generated in a synchronous manner.

Fig. 6 demonstrates the schematic diagram of the synchronous control system. The charging circuit includes a transformer and a bridge rectifier, which is similar to the charging circuit in the uniaxial symmetric electromagnetic SHB system. A set of six capacitors are connected in parallel to the aforementioned charging circuit. Moreover, each capacitor is regulated by an independent switch. A digital delay generator and a multichannel high-voltage pulse trigger are employed in conjunction to generate independent pulses and to trigger the thyristors along each axis. This enables the digital delay generator to control the launch time of the stress pulse along each loading direction. To guarantee the synchronization accuracy of true triaxial impact loading is within 5 μs, a DG645 digital delay generator with time accuracy of nanoseconds is applied.

Once the selected capacitors have reached their target charge during the testing phase, the digital delay generator will then output the requisite triggering signals for the multichannel

high-voltage pulse trigger at the designated time. The trigger then synchronously commands the opening of the thyristors in the selected branches. Subsequently, the discharge currents are generated and flow into the ESPGs, where stress pulses are synchronously generated via electromagnetic conversion. Ultimately, the stress pulses are transmitted into the Hopkinson bars as the incident pulses, as shown in Fig. 2.

The synchronous discharge control system allows for the precise generation of electromagnetic stress pulses in a synchronous manner, thereby enabling multi-axial and multi-directional synchronous impact loading with a time discrepancy of less than 5 μs.

4.1.3 Control System

The coordination of the dynamic triaxial impact loading system requires the implementation of an effective control system. The control system is composed of three principal components: the human-machine interface (HMI) system, the charging and discharging system and the dynamic testing system, as shown in Fig. 7. During service, the HMI system shows the current status of the entire system in real time and translates manual inputs into digital signals. These signals are then conveyed to the charging and discharging system, which initiates the charging or discharging of the capacitor bank. Upon discharging, the capacitor bank's voltage is transferred to the dynamic testing system, where it is transformed into electromagnetic energy and ultimately into the incident wave pulses, which are employed to characterize the dynamic response of the specimen.

The charging and discharging system is a key part of the DTEHB. Upon issuance of a charging command by the HMI system to the programmable logic controller, the charging trigger will establish a connection between the capacitor bank and the capacitor charging circuit. Meanwhile, the voltage and current transmitters convert the real-time voltage and current of the capacitor bank into analog data. Then, the data are transferred to the programmable logic controller by the Analog I/O module. The programmable logic controller can monitor the voltage and current of the capacitor bank in real time. A safety monitor is employed to prevent damage to the system in emergency cases. For instance, in the event that the capacitor bank is overcharged or the charging rate exceeds a specified threshold, the programmable logic controller will transmit a termination signal to the charging circuit, which will then immediately terminate the charging process for the capacitor bank. Upon receipt of a discharging signal from the HMI system, the programmable logic controller

initiates a connection with the capacitor discharging circuit, thereby enabling the capacitor bank to discharge to the ESPGs, which in turn trigger the dynamic testing system. In the event of an emergency, the programmable logic controller is capable of directly releasing the electric energy stored in the capacitor bank directly to the ground via the leakage trigger, thus safeguarding the entire system.

4.2 Static Triaxial Pressure Loading System

In an axisymmetric triaxial confined SHB apparatus, the static confining stress state ($\sigma_1 \geqslant \sigma_2=\sigma_3\neq 0$) differs from the *in-situ* stress condition ($\sigma_1 \geqslant \sigma_2 \geqslant \sigma_3 \neq 0$). To address this technical challenge, a servo-controlled static triaxial pressure loading system has been developed. The static triaxial pressure loading system is mainly comprised of a triaxial frame, a set of specially designed bars and a servo-controlled hydraulic pressure loading system. It is essential that the servo control system maintains a relatively stable static confining pressure during the dynamic loading process.

4.2.1 Triaxial frame

As shown in Fig. 1, the loading frame is an orthogonally triaxial system. The supporting frame is constructed from alloy steel (42CrMo) through precision manufacturing, exhibiting high rigidity and high strength. The triaxial frame not only bears the weight of the entire system, but also provides a high-precision datum for the system.

4.2.2 Square bars

The bar component is composed of six square bars with a dimension of 50×50×2800 mm^3. To avoid the effect of electromagnetic interference on strain signal detection, the square bar is made of anti-magnetic titanium alloy with high yield strength (approximately 1050 MPa). To prevent the stress wave from dispersing or oscillating within the square bars, the straightness of the square bars is limited to a maximum deviation of 0.1‰, and their surfaces are carefully ground to achieve a maximum polishing flatness of 0.8. As the incident end of the square bar is directly in connect with the ESPG, and the pulse generator cannot withstand prestress, it is not possible to apply the static confining pressure directly to the incident end of the bar. To address this technical challenge, a circular bulge is incorporated at a distance of 150 mm from the incident end of the square bar, as shown in Fig. 8. The diameter and thickness of the circular bulge are 90 mm and 70 mm,

respectively. In this way, the static pressure is applied to the circular bulge. The static confining stress is provided by the servo-controlled hydraulic pressure system, as illustrated in Fig. 8. Hence, the static confining pressure of the test specimen is applied via the circular bulge and the bar.

The servo-controlled hydraulic pressure system is composed of a hydraulic pump station, three hydraulic cylinders and a servo control system. The maximum confining pressure and the precision are designed to be 300 MPa and 0.5 MPa, respectively. Fig. 8 illustrates a schematic diagram of the application of static confining pressure along one axis. The servo-controlled hydraulic pressure system along one axis is primarily comprised of a hydraulic cylinder, a benchmark box, support frames, two confining pressure loading frames and two square bars. With the exception of the confining pressure loading frames and the square bars, all of the supporting parts are screwed into an integrated frame. During service, the test specimen is sandwiched between two square bars. One side of the frame (the right side for the illustration in Fig. 8) is set as a fixed end, while the other side is designated as the confining pressure loading end. The hydraulic pump station drives the piston inside the hydraulic cylinder to move, thus exerting force on the confining pressure loading frame and causing it to contact with the circular bulge. As the piston gradually shifts to the right, the confining pressure loading frame gradually applies the axial load exerted by the hydraulic cylinder to the test specimen via the circular bulge and the square bar on the right side of the circular bulge. Notably, because the right side of the frame is fixed, the right square bar and the right surface of the test specimen remain stable during the entire loading process. Upon reaching the desired confining pressure, it is maintained for the subsequent dynamic impact. During dynamic loading, the static confining pressure remains relatively stable to avoid the rise of the confining pressure induced by the Poisson's effect.

5. Verification and Testing

To examine whether the aforementioned functions and performances have been achieved, some verification tests have been carried out on the DTEHB.

5.1 Adjustability of stress wave duration

Fig. 9 illustrates the incident stress waves with varying durations generated by the ESPG. By switching the capacitance of the capacitor bank, for instance, from 1 mF to 4 mF, it is possible to

generate an incident stress wave with a pulse duration ranging from 400 to 800 μs, as illustrated in Fig. 9a. Notably, the power stored in a capacitor bank is dependent on both the charging voltage and the capacitance of the capacitor, as illustrated in Eq. (9). Therefore, it is necessary to adjust the charging voltage in order to generate incident stress waves with a consistent amplitude but varying pulse durations for different capacitances. Figure 9a also illustrates that the duration of the stress wave can be shortened to approximately 300 μs by decreasing the number of turns of the copper strips from 16 to 8. This is due to the inverse relationship between the number of turns and the inductance of the active coil. As the number of turns is reduced, the inductance of the coil is also reduced, resulting in a shorter duration of the stress wave. Conversely, an increase in the number of turns results in an increase in the duration of the stress wave.

5.2 Adjustability of stress wave amplitude

Fig. 10a demonstrates the results of modifying the amplitude of the stress wave by adjusting the charging voltage while maintaining the capacitance at 4 mF. By maintaining the capacitance at a constant level and increasing the charging voltage from 1500 V to 4000 V, we can regulate the amplitude of the stress wave from 100 MPa to 600 MPa while maintaining the stress wave duration at approximately 725 μs, thus meeting the requirements of different tests on the amplitude. It should be noted that the amplitude of the stress wave can also be regulated by modifying the capacitance and the number of turns of the active coil (see Fig. 10b). Therefore, through a comprehensive adjustment of the capacitance, voltage, and the number of turns of the active coil, the requisite test conditions for varying stress wave durations and amplitudes can be satisfied.

5.3 Repeatability of stress waves

The ability to reproduce and replicate experimental results is contingent upon the repeatability of incident stress waves. Fig. 11 illustrates the results of repeated generation of the incident stress waves by the same ESPG (the capacitance of the active coil is 2 mF, and the number of turns of copper tape is 12) at two distinct voltages (i.e., 1500 V and 2000 V, respectively). As illustrated in Fig. 11, the incident stress wave generated by the electromagnetic conversion technology exhibits high levels of repeatability in terms of both the amplitude, the shape and the duration of the stress wave, with a repeatability of ≥99%. Therefore, it can be concluded that the use of electromagnetic

conversion technology to directly generate incident stress waves effectively addresses the issue of the inability to generate highly repeated incident stress waves through the traditional mechanical impact of the end of the incident bar by a striker bar.

5.4 Static true triaxial confining pressures

The capacity of the dynamic true triaxial Hopkinson bar to effectively apply true triaxial static confining pressure is a key factor in determining its suitability for conducting research on deep underground rocks under the coupling influence of true triaxial static confining pressure and dynamic true triaxial disturbance. Fig. 12 shows the results of loading true triaxial static confining pressure to the specimen independently from the X, Y and Z axes using a static true triaxial confining pressure loading system. The results indicate that the static true triaxial confining pressure of the DTEHB can be applied independently and smoothly without interfering with each other. Furthermore, the static confining pressure can be maintained stable after reaching the target load, which verifies the effectiveness of the device in applying static true triaxial confining pressure.

5.5 Dynamic true triaxial loading test

To verify the viability and effectiveness of the DTEHB, the dynamic true triaxial loading tests were conducted on coal and sandstone specimens. It needs to be noted that in the event of dynamic true triaxial impact loading, volume compression will inevitably occur as a result of the pre-existing defects being compacted and collapsed. Consequently, a collision of the triaxial square bars will be an unavoidable consequence if the dimensions of the cubic specimen are identical to the cross-section side length of the square bar (50 mm). To prevent a potential collision between the bars, the side length of the specimen is adjusted to be 1 mm longer than that of the square bar. It is noteworthy that the additional 1 mm can prevent the collision of the bars and permit the specimen to deform adequately along each axis (up to 2%), given that the dynamic deformation of brittle rocks is typically less than 1%. To prevent a discrepancy between the side surfaces of the square bars and the specimen, a 0.5 mm chamfer is incorporated at each edge of the cubic specimen.

Fig. 13 demonstrates the results of a typical dynamic true triaxial impact test of a coal specimen. Fig. 13a shows the incident and reflected voltage signals recorded on three orthogonal sets of titanium bars during dynamic true triaxial loading. The results demonstrate that during

dynamic true triaxial loading, the incident stress waves generated by six independent ESPGs reach the six loading surfaces of the cubic coal through the titanium alloy compression bars at highly consistent times (with an error of less than 5 μs), and the waveforms and durations (or pulse widths) of the six incident stress waves are basically the same, exhibiting a negligible error. Furthermore, the peak voltages of the six incident stress waves are essentially identical (with consistency >99%), except that the peak of Z1 is approximately 1.89% greater than those of the other five. This discrepancy is primarily attributable to the fact that the final discharge voltages of the Z1 capacitor is approximately 10 V greater than those of the other ones. The data pertaining to the incident stress waves indicates that the DTEHB is capable of generating multiple identical stress pulses in a synchronous and precise manner, thereby enabling the synchronous loading. Similarly, the waveforms and variation patterns of the six reflected waveforms are also basically consistent, but the differences in the peaks have increased. This is mainly due to the anisotropic characteristics of rocks, which result in differences in the transmission and reflection coefficients of stress waves.

Fig. 13b exhibits the dynamic stress balance at the two sides of the coal specimen along the X, Y and Z axes under dynamic true triaxial compression testing, using the stress waves presented in Fig. 13a. It should be noted that when the stress difference between the two sides of the specimen is less than 5%, the specimen is considered to have reached dynamic stress balance in that direction. The results show that stress balance is well achieved during the loading process, with the duration of stress balance in each axial direction accounting for 63-82% of the total duration of the stress wave. It therefore addresses the stress equilibrium problem encountered in the conventional SHB apparatus.

Fig. 13c shows the dynamic stress-strain curves along the X, Y and Z axes for the dynamic true triaxial impact loading test of the coal specimen. The evolution of the dynamic stress-strain curves in each axial direction is essentially analogous. Following a brief compression phase, the specimen rapidly transitions into the linear elastic stage. After a relatively short period of nonlinear deformation, the stress reaches its peak and the specimen subsequently enters the post-peak rebound unloading phase. Given that the incident stresses in the X, Y, and Z directions are essentially equivalent (as shown in Fig. 13a), the peak stresses along these axes exhibit slight variation. However, the peak strain in the Z direction is larger than that in the X and Y directions, predominantly attributable to the presence of anisotropy in the specimen, which gives rise to a

comparatively larger strain in the Z direction.

6. Conclusions

A novel dynamic true triaxial electromagnetic Hopkinson bar (DTEHB) system has been developed and introduced in this paper. It is composed of a triaxial loading frame, an orthogonal bar set, a dynamic impact loading system, a static confining pressure loading system and a data acquisition and analysis system. The servo-controlled static triaxial confining pressure system can independently apply true triaxial static confining pressure to the test specimen from three orthogonal directions. The electromagnetic energy conversion technique is employed to generate controllable stress pulses with high repeatability and precision. The utilization of the synchronization control technique guarantees that the time error associated with the arrival of multiple incident stress waves at the loaded end face of the specimen does not exceed 5 microseconds. A control system has been implemented to facilitate the effective coordination of the dynamic triaxial impact loading system, thereby ensuring the safe and optimal operation of the DTEHB. The integration of the electromagnetic energy conversion technique and the synchronous control technique allows the DTEHB to achieve true triaxial synchronous impact loading with high precision. Furthermore, the DTEHB is capable of achieving dynamic true triaxial impact and true triaxial static confining pressure coupling loading (to replicate 3D dynamic and static *in situ* stress conditions), which are not achievable with conventional SHB equipment.

The development of the DTEHB provides a cutting-edge dynamic testing platform for systematic study of dynamic behavior of rocks and other materials in accordance with the *in-situ* stress conditions and 3D dynamic disturbances with strain rate ranging from 10^1 s^{-1} to 10^3 s^{-1}. The anticipated findings could facilitate the development of the theory of 3D rock dynamics and be applicable to a variety of rock engineering applications.

Acknowledgements

This research is financially supported by the Program for Guangdong Introducing Innovative and Entrepreneurial Teams (2019ZT08G315) and the National Natural Science Foundation of China (52325404, 51827901).

Supplementary material

A supplementary video is supplied for better understanding of the design, principle, function and some potential applications of the DTEHB, and can be found online at https://doi.org/10.6084/m9.figshare.11473737.v1.

References

Ahrens, T. J. and Rubin, A. M., 1993, "Impact-Induced Tensional Failure in Rock." *J. Geophys. Res. Planets*, Vol. 98, No. E1, pp. 1185-1203.

Cadoni, E. and Albertini, C., 2011, "Modified Hopkinson Bar Technologies Applied to the High Strain Rate Rock Tests," In *Advances in Rock Dynamics and Applications*, edited by Y. X. Zhou, and J. Zhao, 79-104.

Cadoni, E., Meda, A., and Plizzari, G. A., 2009, "Tensile Behaviour of FRC under High Strain-Rate." *Mater. Struct.*, Vol. 42, No. 9, pp. 1283-1294.

Chen, W. W. and Ravichandran, G., 1997, "Dynamic Compressive Failure of A Glass Ceramic under Lateral Confinement." *J. Mech. Phys. Solids*, Vol. 45, No. 8, pp. 1303-1328.

Chen, W. W. and Song, B., 2011, Split Hopkinson Kolsky Bar: Design, Testing and Applications, Springer Science and Business Media.

Doan, M. L. and Gary, G., 2009, "Rock Pulverization at High Strain Rate Near the San Andreas Fault." *Nat. Geosci.*, Vol. 2, No. 10, pp. 709-712.

Fairhurst, C. E. and Hudson, J. A., 1999, "Draft ISRM Suggested Method for the Complete Stress-Strain Curve for Intact Rock in Uniaxial Compression." *Int. J. Rock Mech. Min. Sci.*, Vol. 36, No. 3, pp. 279-289.

Frew, D. J., Forrestal, M. J., and Chen, W., 2001, "A Split Hopkinson Pressure Bar Technique to Determine Compressive Stress-Strain Data for Rock Materials." *Exp. Mech.*, Vol. 41, No. 1, pp. 40-46.

Frew, D. J., Forrestal, M. J., and Chen, W., 2002, "Pulse Shaping Techniques for Testing Brittle Materials with A Split Hopkinson Pressure Bar." *Exp. Mech.*, Vol. 42, No. 1, pp. 93-106.

Gary, G. and Bailly, P., 1998, "Behaviour of Quasi-Brittle Material at High Strain Rate. Experiment and Modelling." *Eur. J. Mech. A. Solids*, Vol. 17, No. 3, pp. 403-420.

Gran, J. K., Florence, A. L., and Colton, J. D., 1989, "Dynamic Triaxial Tests of High-Strength Concrete." *J. Eng. Mech.*, Vol. 115, No. 5, pp. 891-904.

Goldsmith, W., Sackman, J. L., and Ewerts, C., 1976, "Static and Dynamic Fracture Strength of Barre Granite." *Int. J. Rock Mech. Min. Sci.*, Vol. 13, No. 11, pp. 303-309.

Hokka, M., Black, J., Tkalich, D., Fourmeau, M., Kane, A., Hoang, N. H., Li, C. C., Chen, W. W., and Kuokkala, V. T., 2016, "Effects of Strain Rate and Confining Pressure on the Compressive Behavior of Kuru Granite." *Int. J. Impact Eng.*, Vol. 91, pp. 183-193.

Ju, Y., Sudak, L., and Xie, H. P., 2007, "Study on Stress Wave Propagation in Fractured Rocks with Fractal Joint Surfaces." *Int. J. Solids Struct.*, Vol. 44, No. 13, pp. 4256-4271.

Karinski, Y. S., Zhutovsky, S., Feldgun, V. R., and Yankelevsky, D. Z., 2017, "The Equation of State of Unsaturated Cementitious Composites–A New Multiscale Model." *Int. J. Solids Struct.*, Vol. 109, pp. 12-21.

Kolsky, H., 1963, *Stress Waves in Solids*, Courier Corporation.

Kumar, A., 1968, "The Effect of Stress Rate and Temperature on the Strength of Basalt and Granite." *Geophysics*, Vol. 33, No. 3, pp. 501-510.

Kumari, W. G. P., Ranjith, P. G., Perera, M. S. A., Shao, S., Chen, B. K., Lashin, A., Arifi, N. Al., and Rathnaweera, T. D., 2017, "Mechanical Behaviour of Australian Strathbogie Uranite under In-Situ Stress and Temperature Conditions: An Application to Geothermal Energy Extraction." *Geothermics*, Vol. 65, pp. 44-59.

Lambert, D. E. and Ross, C. A., 2000, "Strain Rate Effects on Dynamic Fracture and Strength." *Int. J. Impact Eng.*, Vol. 24, No. 10, pp. 985-998.

Li, J. C., Li, N. N., Li, H. B., and Zhao, J. 2017a. "An SHPB Test Study on Wave Propagation Across Rock Masses with Different Contact Area Ratios of Joint." *Int. J. Impact Eng.*, Vol. 105, pp.109-116.

Li, X. B., Lok, T. S., and Zhao, J., 2005, "Dynamic Characteristics of Granite Subjected to Intermediate Loading Rate." *Rock Mech. Rock Eng.*, Vol. 381, pp. 21-39.

Li, X. B., Zhou, T., and Li, D. Y., 2017b, "Dynamic Strength and Fracturing Behavior of Single-Flawed Prismatic Marble Specimens under Impact Loading with A Split-Hopkinson Pressure Bar." *Rock Mech. Rock Eng.*, Vol. 50, No. 1, pp. 29-44.

Li, X. B., Zhou, Z. L., Hong, L., and Yin, T. B., 2009, "Large Diameter SHPB Tests with A Special Shaped Striker." ISRM News J, Vol. 12, pp. 76-79.

Li, X.B., Zhou, Z. L., Lok, T. S., Hong, L., and Yin, T. B., 2008, "Innovative Testing Technique of Rock Subjected to Coupled Static and Dynamic Loads." *Int. J. Rock Mech. Min. Sci.*, Vol. 45, No. 5, pp. 739-748.

Lindholm, U. S., Yeakley, L. M., and Nagy, A., 1974, "The Dynamic Strength and Fracture Properties of Dresser Basalt." *Int. J. Rock Mech. Min. Sci.*, Vol. 115, pp. 181-191.

Liu, K., Zhang, Q. B., Wu, G., Li, J. C., and Zhao, J., 2019, "Dynamic Mechanical and Fracture Behaviour of Sandstone Under Multiaxial Loads Using a Triaxial Hopkinson Bar." *Rock Mech. Rock Eng.*, Vol. 52, No. 7, pp. 2175-2195.

Lu, Y. B., Li, Q. M., and Ma, G. W., 2010, "Numerical Investigation of the Dynamic Compressive Strength of Rocks Based on Split Hopkinson Pressure Bar Tests." *Int. J. Rock Mech. Min. Sci.*, Vol. 54, No. 7, pp. 829-838.

Luo, W., Chau, V. T., and Bažant, Z. P., 2019, "Effect of High-Rate Dynamic Comminution on Penetration of Projectiles of Various Velocities and Impact Angles into Concrete." *Int. J. Fract.*, Vol. 216, No. 2, pp. 211-221.

Melosh, H. J., Ryan, E. V., and Asphaug, E., 1992, "Dynamic Fragmentation in Impacts: Hydrocode Simulation of Laboratory Impacts." *J. Geophys. Res. Planets*, Vol. 97, No. E9, pp. 14735-14759.

Nemat-Nasser, S., Isaacs, J., and Rome, J., 2000, "Triaxial Hopkinson Techniques." *Materials Park, OH: ASM International,* pp. 516-518.

Nie, H. L., Suo, T., Wu, B. B., Li, Y. L., and Zhao, H., 2018a, "A Versatile Split Hopkinson Pressure Bar using Electromagnetic Loading." *Int. J. Impact Eng.*, Vol. 116, pp. 94-104.

Nie, H. L., Suo, T., Shi, X. P., Liu, H. F., Li, Y. L., and Zhao, H., 2018b, "Symmetric Split Hopkinson Compression and Tension Tests Using Synchronized Electromagnetic Stress Pulse Generators." *Int. J. Impact Eng.*, Vol. 122, pp. 73-82.

Olsson, W. A., 1991, "The Compressive Strength of Tuff as A Function of Strain Rate from 10^{-6} to 10^{3}/sec." *Int. J. Rock Mech. Min. Sci.,* Vol. 28, No. 1, pp. 115-118.

Patton, T. L., Logan, J. M., and Friedman, M., 1998, "Experimentally Generated Normal Faults in Single-Layer

and Multilayer Limestone Specimens at Confining Pressure." *Tectonophysics*, Vol. 295, Nos. 1-2, pp. 53-77.

Peng, K., Liu, Z. P., Zou, Q. L., Zhang, Z. Z., and Zhou, J. Q., 2019, "Static and Dynamic Mechanical Properties of Granite from Various Burial Depths." *Rock Mech. Rock Eng.*, Vol. 52, No. 10, pp. 3545-3566.

Peng, R. D., Ju, Y., Wang, J. G., Xie, H. P., Gao, F., and Mao, L. T., 2015, "Energy Dissipation and Release During Coal Failure under Conventional Triaxial Compression." *Rock Mech. Rock Eng.*, Vol. 48, No. 2, pp. 509-526.

Perkins, R. D., Green, S. J., and Friedman, M., 1970, "Uniaxial Stress Behavior of Porphyritic Tonalite at Strain Rates to 10^3/second." *Int. J. Rock Mech. Min. Sci.*, Vol. 75, pp. 527-535.

Qi, C. Z., Xia, C., Li, X. Z., and Sun, Y. J., 2019, "Effect of Inertia and Crack Propagation on Dynamic Strength of Geologic-Type Materials." *Int. J. Impact Eng.*, Vol. 133, No. 103367.

Ranjith, P. G., Zhao, J., Ju, M., De Silva, R. V., Rathnaweera, T. D., and Bandara, A. K., 2017, "Opportunities and Challenges in Deep Mining: A Brief Review." *Engineering*, Vol. 3, No. 4, pp. 546-551.

Reddish, D. J., Stace, L. R., Vanichkobchinda, P., and Whittles, D. N., 2005, "Numerical Simulation of the Dynamic Impact Breakage Testing of Rock." *Int. J. Rock Mech. Min. Sci.*, Vol. 42, No. 2, pp. 167-176.

Rehbock-Sander, M. and Jesel, T., 2018, "Fault Induced Rock Bursts and Micro-Tremors–Experiences from the Gotthard Base Tunnel." *Tunn. Undergr. Space Technol.*, Vol. 81, pp. 358-366.

Richter, B., Stünitz, H., and Heilbronner, R., 2018, "The Brittle-to-Viscous Transition in Polycrystalline Quartz: An Experimental Study." *J. Struct. Geol.*, Vol. 114, pp. 1-21.

Scott, T. E. and Nielsen, K. C., 1991, "The Effects of Porosity on the Brittle-Ductile Transition in Sandstones." *J. Geophys. Res. Solid Earth*, Vol. 96, No. B1, pp. 405-414.

Song, B. and Chen, W., 2004, "Loading and Unloading Split Hopkinson Pressure Bar Pulse-Shaping Techniques for Dynamic Hysteretic Loops." *Exp. Mech.*, Vol. 44, No. 6, pp. 622-627.

Wang, M., Zhu, Z. M., Dong, Y. Q., and Zhou, L., 2017, "Study of Mixed-Mode I/II Fractures using Single Cleavage Semicircle Compression Specimens under Impacting Loads." *Eng. Fract. Mech.*, Vol. 177, pp. 33-44.

Wang, Q. Z., Li, W., and Xie, H. P., 2009, "Dynamic Split Tensile Test of Flattened Brazilian Disc of Rock with SHPB Setup." *Mech. Mater.*, Vol. 41, No. 3, pp. 252-260.

Wasantha, P. L. and Ranjith, P. G., 2014, "Water-Weakening Behavior of Hawkesbury Sandstone in Brittle Regime." *Eng. Geol.*, Vol. 178, pp. 91-101.

Whittles, D. N., Kingman, S., Lowndes, I., and Jackson, K., 2006, "Laboratory and Numerical Investigation into the Characteristics of Rock Fragmentation." *Miner. Eng.*, Vol. 19, No. 14, No. 1418-1429.

Wu, B. B., Yao, W., and Xia, K. W., 2016, "An Experimental Study of Dynamic Tensile Failure of Rocks Subjected to Hydrostatic Confinement." *Rock Mech. Rock Eng.*, Vol. 49, No. 10, pp. 3855-3864.

Xia, K. W. and Yao, W., 2015, "Dynamic Rock Tests using Split Hopkinson Kolsky Bar System–A Review." *J. Rock Mech. Geotech. Eng.*, Vol. 7, No. 1, pp. 27-59.

Xie, H. P. and Sanderson, D. J., 1996, "Fractal Effects of Crack Propagation on Dynamic Stress Intensity Factors and Crack Velocities." *Int. J. Fract.*, Vol. 74, No. 1, pp. 29-42.

Xie, H. P., Zhu, J. B., Zhou, T., Zhang, K., and Zhou, C. T., 2020, "Conceptualization and Preliminary Study of Engineering Disturbed Rock Dynamics." *Geomech. Geophys. Geo-energ. Geo-resour.*, Vol. 6, pp. 34.

Xie, H. P., Zhu, J. B., Zhou, T., and Zhao, J., 2021, "Novel Three-Dimensional Rock Dynamic Tests using the True Triaxial Electromagnetic Hopkinson Bar System." *Rock Mech. Rock Eng.*, Vol. 54, pp. 2079-2086.

Xu, S. L., Shan, J. F., Zhang, L., Zhou, L. J., Gao, G. F., Hu, S. S., and Wang, P. F., 2020, Dynamic Compression Behaviors of Concrete under True Triaxial Confinement: An Experimental Technique. *Mech. Mater.* Vol. 140, pp. 103220.

Yuan, F. P., Prakash, V., and Tullis, T., 2011, "Origin of Pulverized Rocks During Earthquake Fault Rupture." *J. Geophys. Res. Solid Earth*, Vol. 116, No. B06309, pp. 1-18.

Zhang, Q. B. and Zhao, J., 2013, "Determination of Mechanical Properties and Full-Field Strain Measurements of Rock Material under Dynamic Loads." *Int. J. Rock Mech. Min. Sci.*, Vol. 60, pp. 423-439.

Zhang, Q. B. and Zhao, J., 2014, "A Review of Dynamic Experimental Techniques and Mechanical Behaviour of Rock Materials." *Rock Mech. Rock Eng.*, Vol. 47, No. 4, pp. 1411-1478.

Zhao, H. and Gary, G., 1996, "On the Use of SHPB Techniques to Determine the Dynamic Behavior of Materials in the Range of Small Strains." *Int. J. Solids Struct.*, Vol. 33, No. 23, pp. 3363-3375.

Zhao, J. and Cadoni, E., 2009, "Triaxially Compressed Hopkinson Bar (TriHB) for Geomaterial and Construction Material Testing." Proposal Submitted to the Swiss National Science Foundation (SNSF), No. 206021_128734, EPFL, Switzerloand.

Zhao, J., et. al., 2015, "Three Dimensionally Compressed and Monitored Hopkinson Bar," Australian Research Council, ARC LIEF (No. LE150100058), granted in 2016, Monash University, Australia.

Zhou, Y. X., Xia, K. W., Li, X. B., Li, H. B., Ma, G. W., Zhao, J., Zhou, Z. L., and Dai, F., 2012, "Suggested Methods for Determining the Dynamic Strength Parameters and Mode-I Fracture Toughness of Rock Materials." *Int. J. Rock Mech. Min. Sci.*, Vol. 49, pp. 105-112.

Zhou, T., Dong, S. L., Zhao, G. F., Zhang, R., Wu, S. Y., and Zhu, J. B., 2018, "An Experimental Study of Fatigue Behavior of Granite under Low-Cycle Repetitive Compressive Impacts." *Rock Mech. Rock Eng.*, Vol. 51, No. 10, pp. 3157-3166.

Zhou, T., Zhu, J. B., and Xie, H. P., 2020, "Mechanical and Volumetric Fracturing Behaviour of Three-Dimensional Printing Rock-Like Samples under Dynamic Loading." *Rock Mech. Rock Eng.*, Vol. 53, pp. 2855-2864.

Zhu, J. B., Liao, Z. Y., and Tang, C. A., 2016, "Numerical SHPB Tests of Rocks under Combined Static and Dynamic Loading Conditions with Application to Dynamic Behavior of Rocks under In Situ Stresses." *Rock Mech. Rock Eng*., Vol. 49, No. 10, pp. 3935-3946.

Zhu, J. B., Zhou, T., Liao, Z. Y., Sun, L., Li, X. B., and Chen, R., 2018a, "Replication of Internal Defects and Investigation of Mechanical and Fracture Behaviour of Rock using 3D Printing and 3D Numerical Methods in Combination with X-Ray Computerized Tomography." *Int. J. Rock Mech. Min. Sci.*, Vol. 106, pp. 198-212.

Fig. 1 Dynamic true triaxial electromagnetic Hopkinson bar

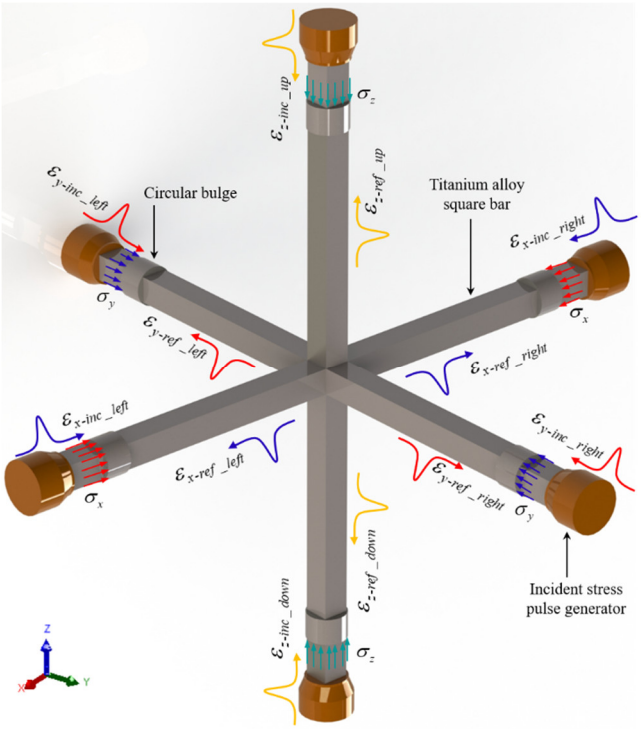

Fig. 2 Schematic diagram of stress state and wave propagation in the triaxial bars

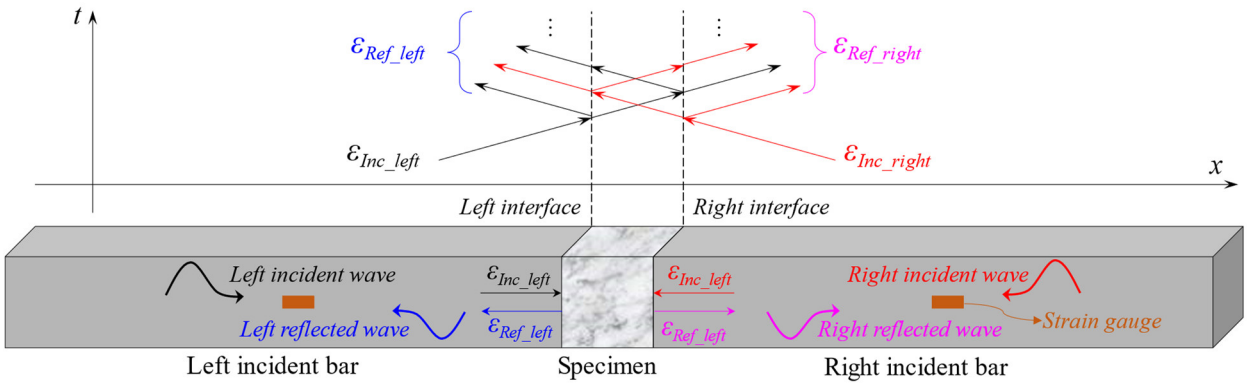

Fig. 3 Schematic diagram of the propagation of waves along the *x*-axis under conditions of symmetric loading

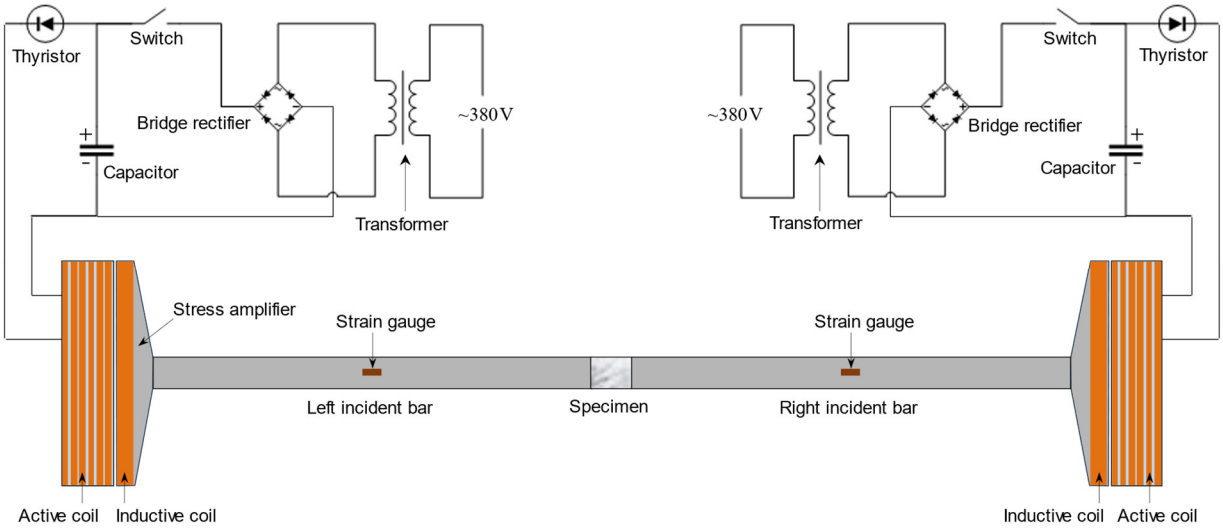

Fig. 4 Schematic diagram of the electromagnetic stress pulse generation system in each axis

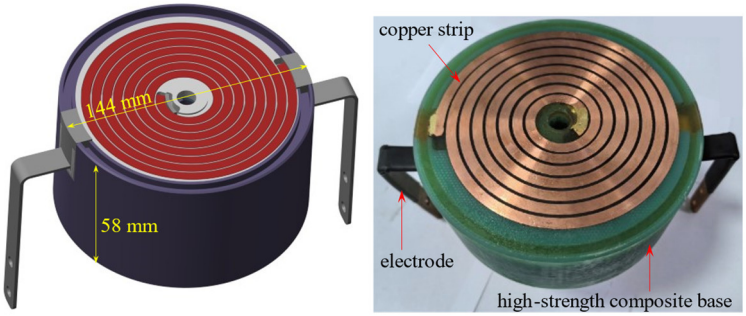

Designed active coil Machined active coil

Fig. 5 3D structure of an active coil

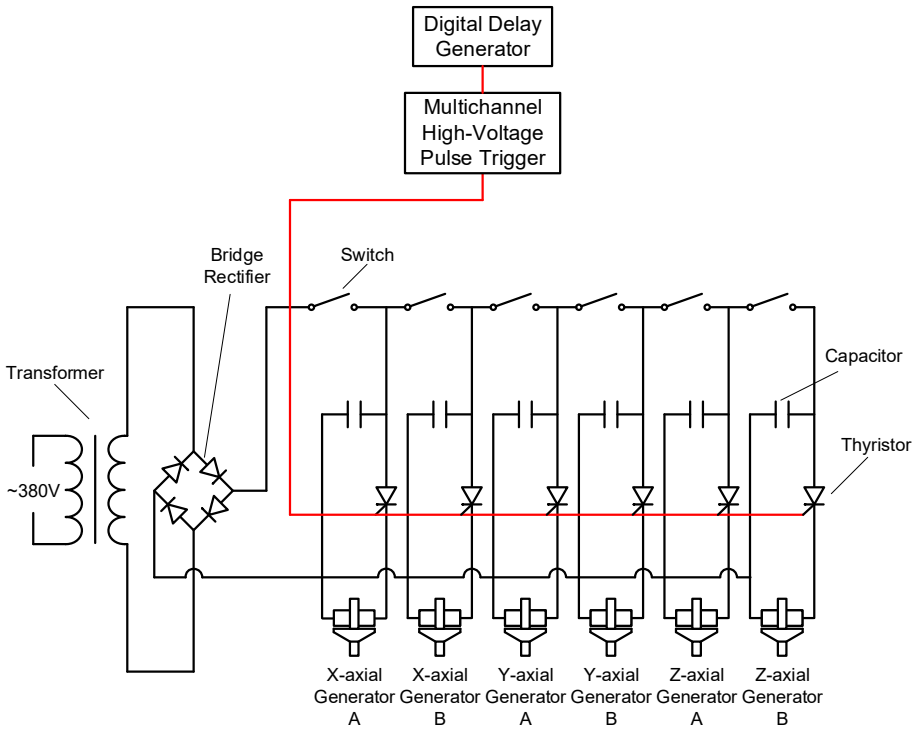

Fig. 6 Schematic diagram of the synchronous control system

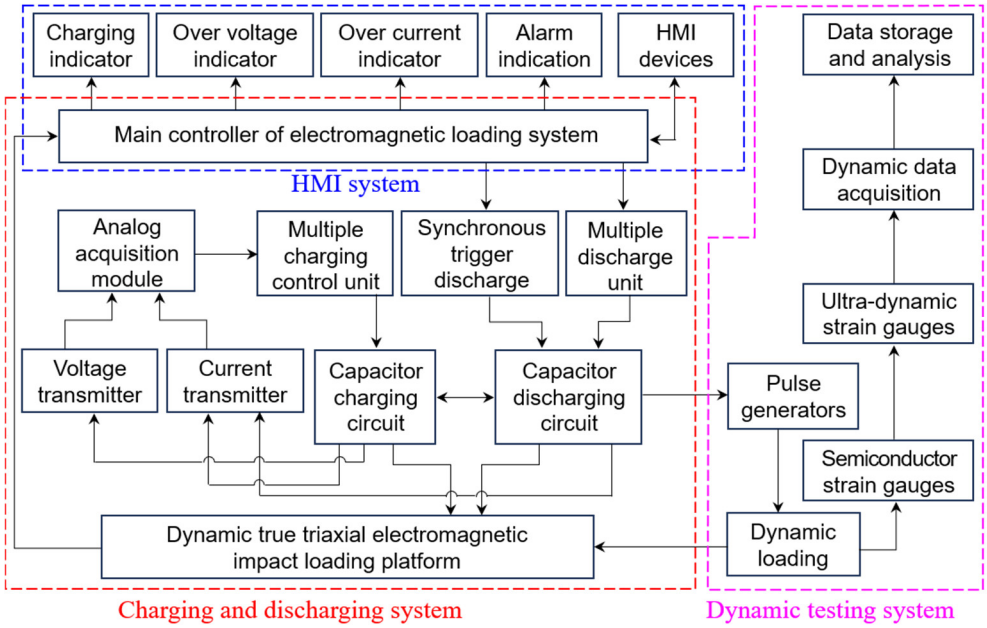

Fig. 7 Principle of the control system

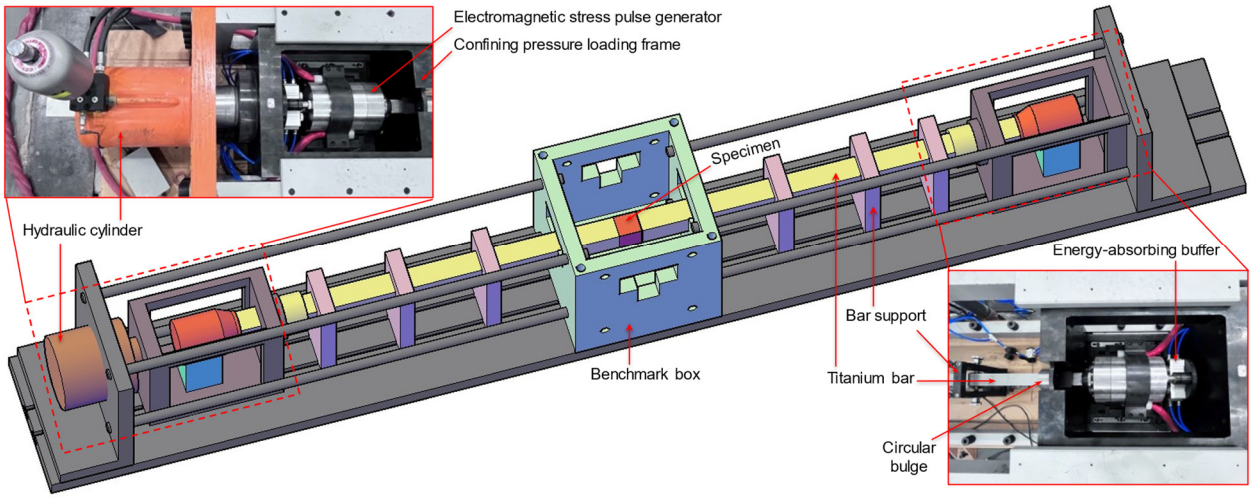

Fig. 8 Triaxial frame and static confining pressure loading system in one axis

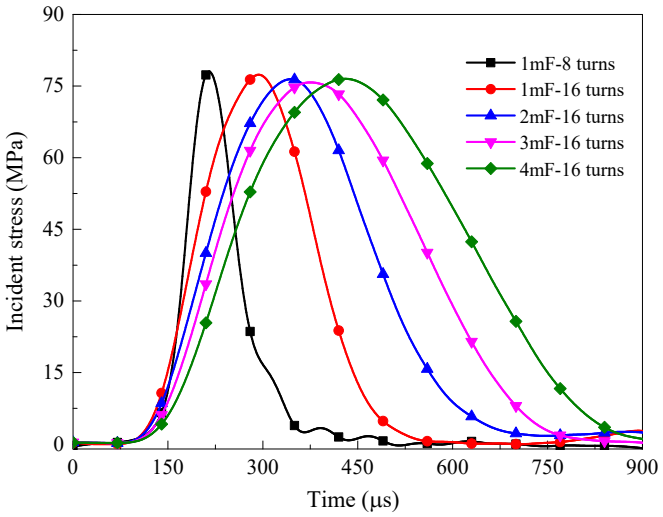

Fig. 9 Controllable and adjustable of stress wave durations generated by the ESPG

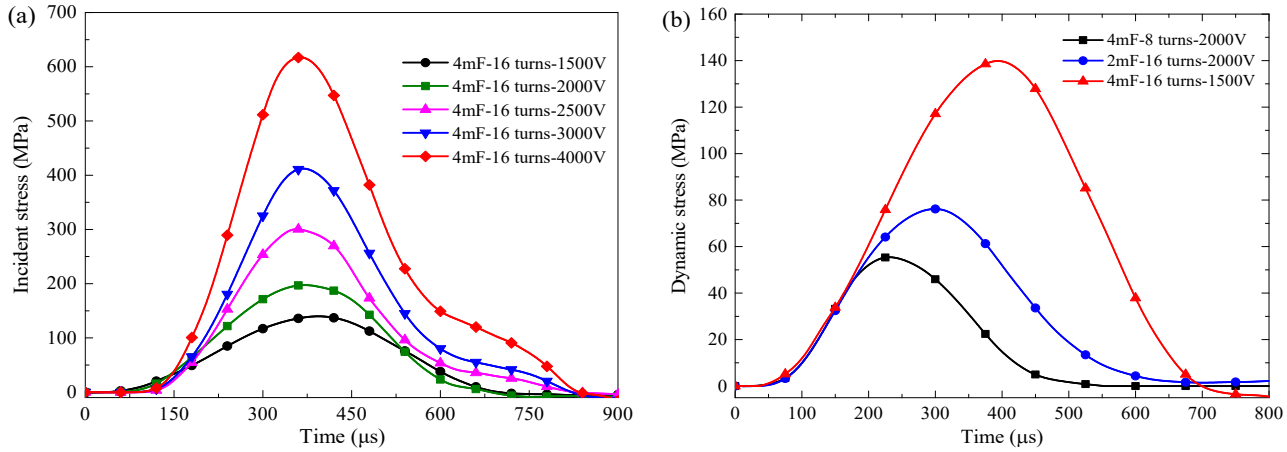

Fig. 10 Controllable and adjustable of stress wave amplitudes generated by the ESPG. (a) Effect of charging voltages on the amplitude; (b) Effect of capacitances and the numbers of turns of the active coil on the amplitude.

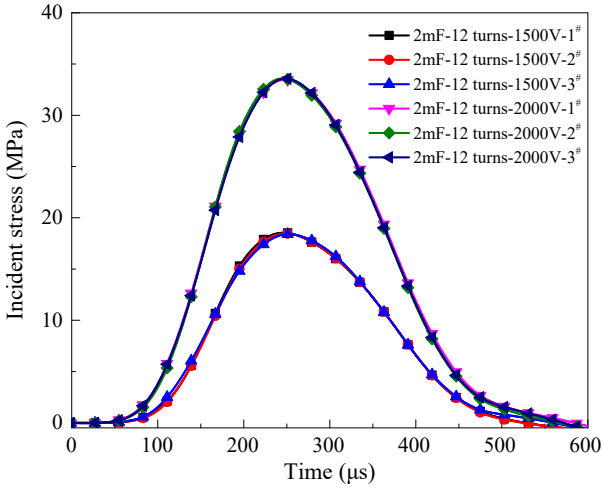

Fig. 11 Repeatability of stress waves generated by the ESPG

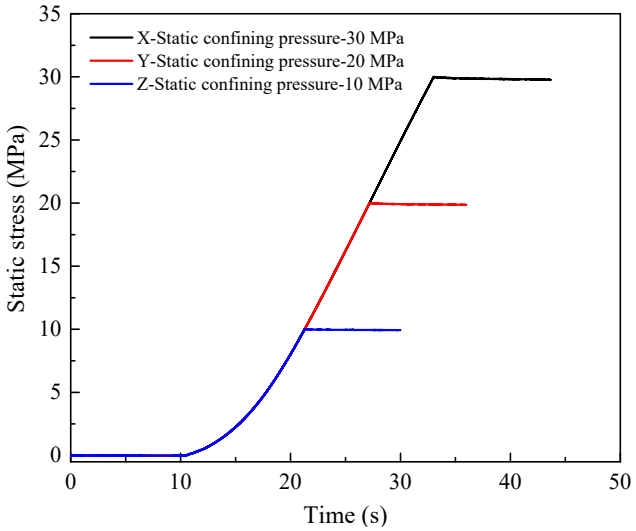

Fig. 12 Application of static confining pressures along each axis

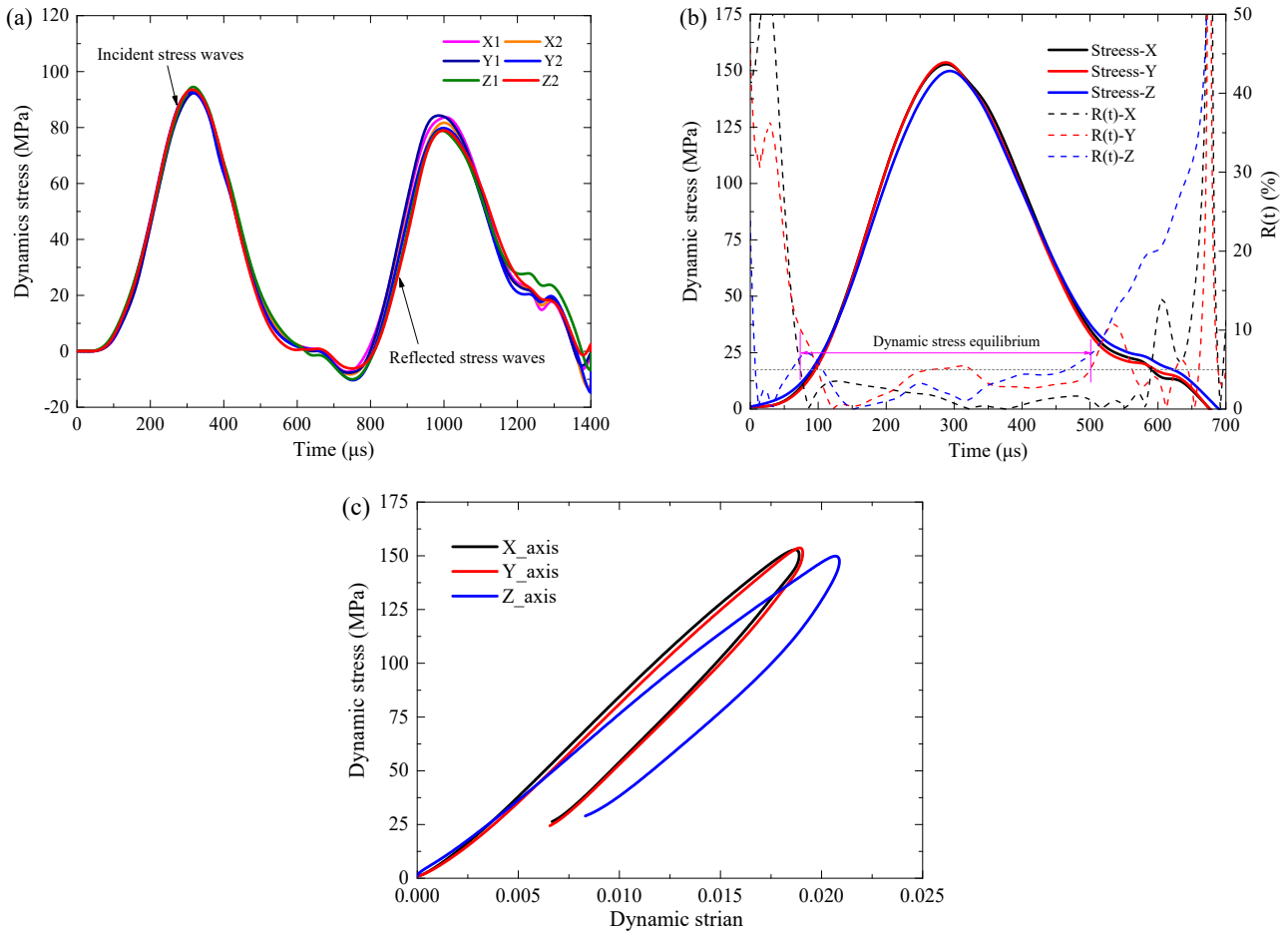

Fig. 13 A typical dynamic true triaxial impact test of a coal specimen. (a) Incident strain signals measured on the triaxial bars; (b) force balance in each axis; (c) dynamic stress-strain curves in the X, Y and Z axes of the coal specimen.

Table 1 Summary of the techniques, equipment and objectives for data acquisition and analysis

Signals	Technique	Equipment	Objectives
Dynamic strain	Synchronous signal acquisition technology	Multi-channel dynamic strain recorder	Dynamic stress-strain curves, equivalent stress-equivalent stain curves; dynamic mechanical properties, e.g., dynamic strength and strain,
Surface fracturing	High-speed photogrammetry	Ultra-high-speed camera	Crack propagation velocity; crack nucleation, initiation, propagation, coalescence, termination and failure modes
3D fracturing, deformation	High-speed photogrammetry, 3D DIC technique	High-speed cameras, DIC analysis software	3D fracturing type, behavior and mechanism; full field deformation and its localization and evolution
Acoustic emission (AE)	AE detection technology	AE probe, AE detector	Spatial and temporal evolution of damage as well as fracturing process inside the specimen
Macro- and meso-cracks	X-ray computed tomography (CT)	High-resolution X-ray CT	2D and 3D damage and fracture network inside opaque materials; spatial evolution of micro- and macro-crack inside the specimen
Meso- and micro-cracks	Scanning electron microscope	Scanning electron microscope	Microcrack characteristics; failure mechanism of the specimen at microscopic scale